Fuel 333 (2023) 126266

Contents lists available at ScienceDirect

Fuel

journal homepage: www.elsevier.com/locate/fuel

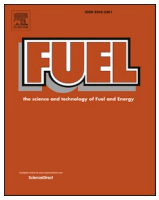

Evaluation of the effect of pressure and heat transfer on the efficiency of a batch fuel reactor, using Iron-based Oxygen Carrier with a CFD model

Wang Lu [a], Pietro Bartocci [b,*], Alberto Abad [b], Arturo Cabello [b], Margarita de Las Obras Loscertales [b], Teresa Mendiara [b], Liang Wang [c], Qi Chen [a], Yingquan Chen [a], Xianhua Wang [a], Haiping Yang [a,*], Hanping Chen [a], Mauro Zampilli [d], Francesco Fantozzi [d]

[a] State Key Laboratory of Coal Combustion, Huazhong University of Science and Technology, Wuhan, China
[b] Instituto de Carboquímica (ICB-CSIC), Miguel Luesma Castán 4, 50018 Zaragoza, Spain
[c] SINTEF Energy Research, Postboks 4761, Torgarden, Trondheim, Norway
[d] Department of Industrial Engineering, University of Perugia, Via G. Duranti 67, 06125 Perugia, Italy

ARTICLE INFO

Keywords:
Chemical looping combustion
Syngas
Iron
BECCS
Bioenergy
Gas turbine

ABSTRACT

Coupling a Chemical Looping Combustor fed with biofuels with a turbo expander is a promising Negative Emissions Technology (NET) to realize climate neutral targets in China and Europe. This is also an example of Bioenergy with Carbon Capture and Storage (BECCS) technology. To realize it, we need a Pressurized Chemical Looping Combustion process (PCLC). In this work, a Eulerian-Lagrangian hybrid model is developed in Barracuda-VR^{TM} software, incorporating chemical reactions to predict the performance of a Fuel Reactor using Fe_2O_3 as oxygen carrier and syngas as fuel, under different pressures, ranging from 1 bar to 20 bars. The model predicted the conversion efficiency of syngas reduction using an iron-based oxygen carrier (Fe_2O_3/Al_2O_3). The results show, that the increase in pressure promotes the conversion of CO and inhibits the conversion of H_2. When the two gases are considered together, the increase in pressure promotes the reaction between syngas and Fe_2O_3 and reduces the demand for Fe_2O_3 oxygen carrier per unit of syngas Lower Heating Value and so also the inventory of the reactor. Increasing temperatures promotes both the reaction of H_2 and CO with Fe_2O_3. Dealing with CO conversion, this is more affected by pressure changes and temperature changes than H_2. This represents important information for Fuel Reactor design, scale up and optimization. Further validation is neded in batch and continuous pressurised plants.

1. Introduction

The power sector is undergoing drastic changes owing to the demand of low carbon technology [1,2]. The "European Green Deal", released by the European Commission, aims at making Europe the first "climate neutral" continent and the first to achieve carbon neutrality by 2050, demonstrating a strong willingness to lead the world in achieving carbon neutrality [3]. The roadmap that has been development in 2019 proposes to realize a 50 % reduction of the EU's greenhouse gas emissions by 2030 (respect to the emissions of year 1990) [4]. To achieve this ambitious goal, it's likely that the conventional gas turbines and internal combustion engines will need to be integrated in systems employing biofuels, alternative fuels (like hydrogen or ammonia) and/or CCS (Carbon Capture and Storage) [5].

CCS is an important process that can significantly reduce CO_2 emissions from industrial activities and power plants and can allow using current combustion based electricity production technologies [6]. On the other hand, CCS can correspond to an energy penalty and so to a reduced efficiency of the power plants, for this reason high efforts in research are focused on developing CCS with the lowest energy penalty (also taking into account that CO_2 to be stored needs to be compressed and liquefied and this will also imply an energy penalty, which is not avoidable).

The IPCC (Intergovernmental Panel on Climate Change) has reported that BECCS (Bioenergy with Carbon Capture and Storage) is a key technology for meeting the carbon reduction targets which have been pledged by the "Paris Agreement" for this century [7]. However, the

* Corresponding authors.
E-mail addresses: pbartocci@icb.csic.es (P. Bartocci), yhping2002@163.com (H. Yang).

https://doi.org/10.1016/j.fuel.2022.126266
Received 13 August 2022; Received in revised form 22 September 2022; Accepted 7 October 2022
Available online 20 October 2022

Nomenclature

Greek letters

∂, ∇, δ	Incremental change, -
θ	Volume fraction, -
μ	Viscosity, kg/(m·s)
ρ	Density, kg/m^3
τ	Stress tensor, Pa
$\varnothing$	Viscous dissipation, -

Subscripts

f	Fluid phase, -
i	The ith species, -
s	Solid phase, -

Symbols

A	Particle acceleration, m/s^2
d	Stoichiometric factor for the combustion of fuel gas with oxygen, mol of O_2 per mol of fuel gas
D	Turbulent mass diffusion coefficient for gas, m^2/s
D_s	Interphase momentum transfer coefficient, -
F	Inter-phase momentum transfer rate
FR	Fuel Reactor, -
h	Specific enthalpy, J/kg
k_0	Pre-exponential constant, -
m	mass, kg
MP-PIC	Multiphase-Particle in Cell, -
n	reaction order, -
OC	Oxygen Carrier, -
p	pressure, Pa
q	Fluid heat flux, W/m^2
R	Universal gas constant, J/(mol·K)
S_h	Inter-phase energy exchange rate, -
V	volume, m^3
T	temperature, K
u	Velocity vector, m/s
Y_i	Mass fraction, -

high cost of the initial investment and the costs of operation are important bottlenecks for the CCS technology to be applied in industrial clusters [8]. CLC (Chemical Looping Combustion) is an attractive technology which produces a pure flow of CO_2 and water vapor as exhaust gases of combustion and for this reason is one of the cheapest ways to perform carbon capture [9,10]. In chemical looping combustion the conventional combustion process is divided into two main reactions: the oxygen in the air is first transferred to the oxygen carrier through an oxidation reaction and then the oxygen carrier reacts with the fuel through a reduction reaction. In total one redox cycle is performed during CLC. In this way, the exhaust gases of combustion are almost only composed by CO_2 and H_2O and so it is easy to reach a high purity flow of carbon dioxide and to avoid the drawbacks of oxyfuel combustion, which are:

- the high temperature of combustion (respect to combustion with air);
- the costs of separating oxygen from air.

We have to take into account also that CLC has less exergy destruction respect to conventional combustion, given that the equilibrium temperature for the reduction and oxidation reactions is much closer to the real temperature at which the oxidation and reduction reactions happen; while the equilibrium temperature of combustion is in reality much higher respect to the real combustion temperature (which is allowed by the current properties of the materials used in combustion chambers and boilers) [11]. This will reduce the irreversibility of the combustion process, when chemical looping is used. Also, the costs of separating the CO_2 after combustion from the exhaust gases (the so-called post combustion carbon capture) can be avoided. This is a treatment which has a high cost due to the high concentration of nitrogen in the exhaust gases, and is encountered in case of conventional combustion processes [8,12]. The difficulty in the separation of CO_2 from exhaust gases of combustion increases further if solids fuels, like coal, are combusted, which implies that exhaust gases have an important concentration of contaminants, like sulfur.

Oxygen carriers play an important role in the economic and efficient operation of CLC combustors [13]. The selection of oxygen carriers requires comprehensive consideration of the price, the conversion rate, the loading amount of oxygen, the resistance to attrition and agglomeration [14–16]. Iron based oxygen carriers of synthetic or natural origin oxygen carriers are considered as promising oxygen carriers, due to their sufficiently high oxygen transport capacity during the whole reduction–oxidation cycle [17,18]. However, in the actual chemical looping reactor, real operating conditions have to be considered and it is interesting to understand how these can influence the oxygen transport capacity, which is typical of the different types of oxygen carriers.

Pressure is a key parameter to increase the efficiency of gas turbines [19], together with turbine inlet temperature (TIT). For power plants based on PCLC (Pressured Chemical Looping Combustion), increasing the pressure will also decrease the cost for CO_2 compression storage in the downstream part [20]. PCLC is still on an embryonal stage if we compare it to PCFB reactors, which have already reached commercial scale [21], see the Karita 360 MWe power plant and the Osaki 250 MWe power plant. The barriers which avoid the development of PCLC power plants on a commercial scale are:

- (1) high efficiency oxygen carriers are needed, which can operate at high temperature and high pressure;
- (2) low attrition rate oxygen carriers are needed which can work in extreme conditions;
- (3) kinetics aspects under high pressure and temperature conditions are not known;
- (4) reactor injection system has to be adapted to biofuels;
- (5) the use of the hot air produced from the air reactor in a gas turbine has to be optimized;
- (6) exhausts should be filtered to retain the dust released by oxygen carrier attrition;
- (7) high electrical efficiency of the power system has to be granted together with high fuel conversion in the combustor.

So far, limited work on the behavior of oxygen carriers for PCLC has been made. Jin et al. [22] designed and manufactured an elevated-pressure (up to 9 bars) fixed-bed reactor and characterized the oxygen carriers in TGA and fixed-bed reactor. Wolf et al. [23] analyzed the feasibility of a CLC system consisting of two interconnected pressurized fluidized bed reactors and further developed the hypothetical layout, by dimensioning its components. Rana et al. [24] analyzed the oxidation performance of ilmenite under pressurized conditions (8 bars) in TGA. They indicated that the oxidation kinetics can be modelled by a two-step mechanism (2nd order random nucleation dominating at lower conversions, and Jander's solid state diffusion model [25] dominating at higher conversions). Our previous study analyzed the influence of pressure and the reduction rates of the oxygen carriers in PTGA experiment [26]. However, the reaction rate between fuel and OCs is not only influenced by OCs' reaction kinetics, but also is favored by the heat and mass transfer, which is a non-negligible factor in industrial PCLC

fluidized bed conditions. Therefore, it's necessary to explore the reaction rate and the detailed behavior of the OC in the fluidized bed fuel reactor under pressured conditions, which is also important for industrial design and optimization of PCLC. Given that Pressurized Chemical Looping combustion (PCLC) pilot plants are still not so common, the use of CFD (Computational Fluid Dynamic) is needed to model and foresee how the technology works and also to design optimized plants.

CFD simulation of the fuel reactor is a useful step to design, optimize, scale up and further understand the performance of industrial equipment [27,28]. The Eulerian-Eulerian (E-E) method and the Eulerian-Lagrangian (E-L) method have been widely used in fuel reactor simulation [29]. Wang et al. [30] investigated the CLC processes in a dual circulating fluidized bed (DCFB) reactor by E-E method. The gas–solid flow behavior and reactive characteristics were well predicted based on a cluster structure-dependent (CSD) drag coefficient model. Li and Shen [31] studied gas–solid hydrodynamics in a 3D DCFB based on E-E method, and predicted reasonable radial solid distribution and pressure distribution using 4 different drag force models. The authors have published a work on a batch fluidized bed reactor fed with biomethane and working with iron-based oxygen carriers [32]. Nevertheless, the performance of the batch fluidized bed and the reaction characterizations of OCs have never been studied in pressurized conditions. Compared with the Eulerian-Eulerian method, the Eulerian-Lagrangian method can track particles in time and space, which greatly improves the calculation accuracy of particle size, density and shape [33]. MP-PIC (multiphase-particle in cell) is a typical Eulerian-Lagrangian method, in which the gas phase is treated as a continuous phase and it is solved using the Eulerian method, while the solid phase is treated as a discrete phase solved by the Lagrangian method [34]. In the MP-PIC method, the concept of parcels is introduced, to simplify the computational costs of the actual calculation process, several particles with same properties (species, temperature, velocity, etc.) are put into a parcel, which represents the calculation unit [35]. This greatly reduces the cost of calculation and improves the efficiency of the model.

Barracuda-VR^{TM} uses the multiphase-particle in cell (MP-PIC) method to simulate gas–solid interactions. This has already been described by Reinking et al. [36]. In this work, we use Barracuda-VR^{TM} (Version 17.4.0) to develop a comprehensive three-dimensional numerical model for the fuel reactor. The reactor is a part of the GTCLC-NEG concept (shown in Fig. 1), which has been proposed in the Marie Curie IF project with the same name.

The project is managed by ICB (Instituto de Carboquimica), belonging to CSIC (Spanish National Research Council). The objective is to develop a Carbon Negative Technology, capable to burn multiple biofuels derived from biomass (eg, pyrolysis oil, biogas and syngas) and to capture the CO_2 emissions at a very low cost. The model incorporates the fluid dynamics, the mass and heat transfer equations, and the chemical reactions that guide the oxygen carrier reduction. Calculations results are compared with the data derived from PTGA experiments performed in ICB-CSIC previous projects, to validate the model. This study has the ultimate objective to investigate the specific behavior of the Fe-based oxygen carrier in the FR and the detailed influence of pressure and temperature under elevated pressure conditions on the oxygen carrier reaction rate.

To the best of authors' knowledge there is no work, at the moment, on CFD of pressurized CLC Fluidized Bed reactors. Besides this, the oxygen carrier used is iron based, but has a high reactivity, due to the influence of Alumina and also this represents an original aspect.

2. Model development

The model simulates the chemical reactions happening in a bubbling fluidized bed reactor, used as a fuel reactor in a chemical looping combustion plant. The set of reactions used in the model are the following:

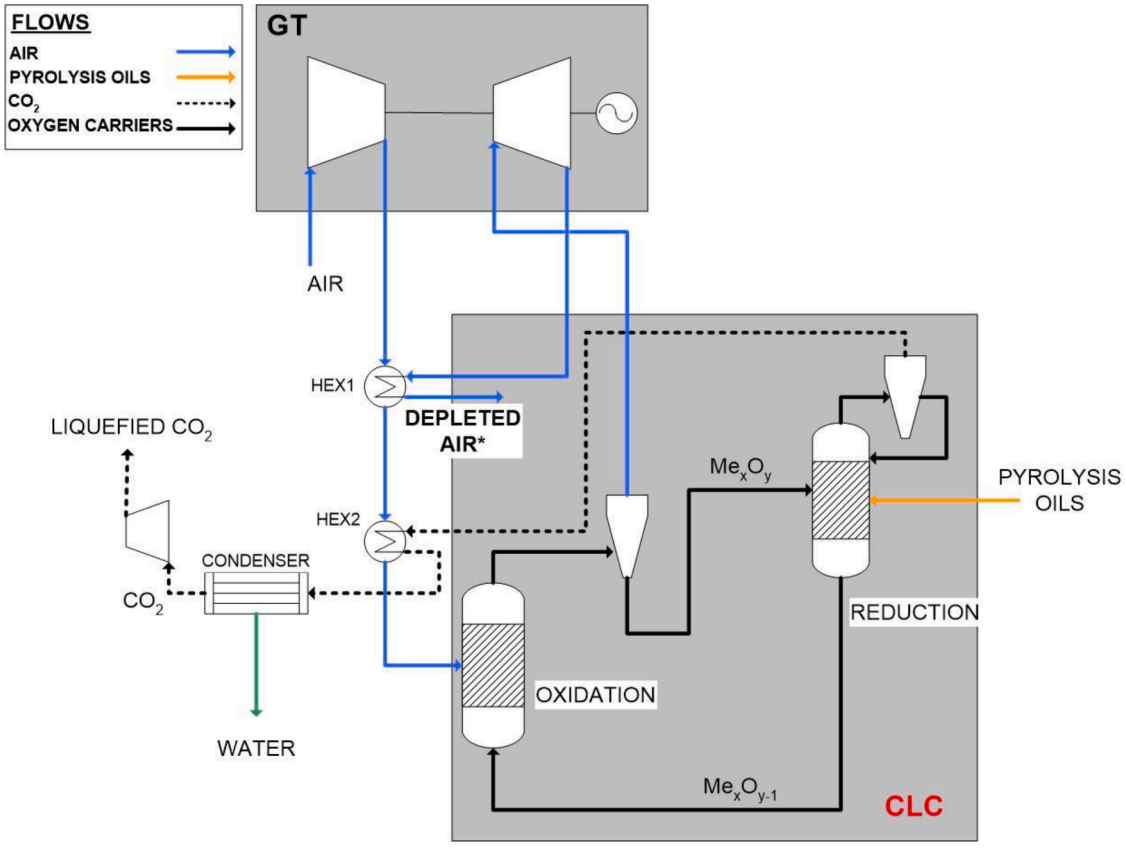

Fig. 1. The GTCLC-NEG concept [32].

$CO + 3\ Fe_2O_3 \rightarrow CO_2 + 2\ Fe_3O_4$ (1).

$H_2 + 3\ Fe_2O_3 \rightarrow H_2O + 2\ Fe_3O_4$ (2).

The transformation of Fe_2O_3 into Fe_3O_4 and then into FeO is regulated by time, as we can see also by [37]. For this reason, it is important to regulate the length of the reduction cycle in a way that it stops once the first reduction of iron is completed. One of the important results of our analysis is to identify the length of the reduction cycle, to stop this before FeO is formed. Future experimental tests will be performed before the cycle ends to derive information also on the kinetics of the process and to confirm in the end the results of the PTGA experiments.

The reactions (1) and (2) are used to model the reduction of the oxygen carrier by two kinds of fuels: CO and H_2. Syngas composition is modelled assuming 50v% of concentration of H_2 and 50v% of concentration of CO, according to what reported also in: [38,39]. The reforming of water vapor over the iron oxygen carrier it is neglected because this phenomenon is much more prevalent when nickel oxygen carrier is used, respect to iron oxygen carrier.

Table 1 shows the different cases that were simulated. As reported in Table 1, the influence of pressure and temperature are studied. The conversion rates of the oxygen carrier using H_2 and CO as fuel are compared with PTGA experimental results, to prove the validity of the model.

The simulation is performed in transitory mode for a maximum period of 90 s.

2.1. Description of fuel reactor model

The structure and mesh of Fuel Reactor (FR) model are shown in Fig. 2. To reduce unnecessary calculation work, the temperature control in the reactor is realized based on three aspects:

- the reactor wall is supposed to be initialized to the desired temperature and to maintain it constant during the reaction process (reactor temperature is changed between 973 K and 1273 K);
- the temperature of the fuel gas entering the reactor is the same as that of the reactor walls;
- the temperature of the solids is the same as that of the reactor walls and of the fuel gas entering the reactor.

In this way the model starts at time 0 when thermal equilibrium is already reached. The inner diameter and the length of the Fuel Reactor are respectively 56 mm and 470 mm. Dealing with the ratio between height and diameter, which is a characterizing parameter in many fluidized bed reactors; we have to consider that the process of chemical looping in fluidized beds needs more stringent conditions respect to gasification and combustion. In fact, for pilot scale CLC reactors, the diameter depends directly from the mass flow (of fuel in this case) and the required velocity range. In fact, we know that the air reactor is usually designed to work in fast fluidization regimes and the fuel reactor is usually designed to work in bubbling fluidization regime, see Fig. 3.

The inlet is located at the bottom of FR, which is set in Barracuda to: flow boundary. As it can be seen from Fig. 3 the velocity used in this study is about 0.3 m/s as it is also indicated in Fig. 4. The choice was done to grant fast and full conversion of the oxygen carrier, based on the height (and so the mass) of the bed material, and also to grant similar operating conditions respect to the experimental tests performed using the PTGA.

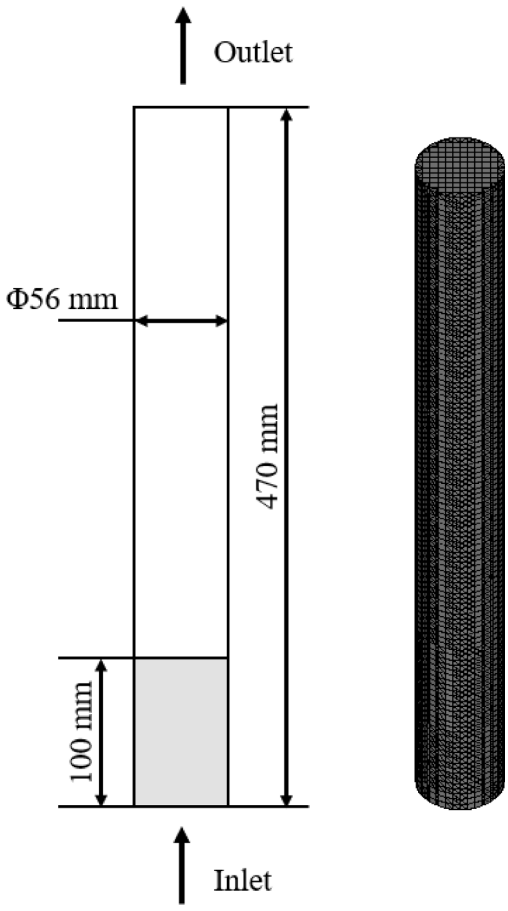

Fig. 2. Geometry and mesh of FR.

Dealing with the height of the reactor, this depends from the Transport Disengaging Height (TDH). Since we don't want entrainment of the oxygen carrier in the Fuel Reactor, the height of the reactor should be at least higher than the TDH.

Dealing with laboratory reactors the dimensions (diameter and height) are mainly given by the dimensions of the heaters. Based on these assumptions, it is the mass flow of the gas which is adapted, always to have the same velocity regimen and the same conditions as experimented in the PTGA reactor.

To reduce the requirements on calculation power, the grid of the model was designed with 20,000 cells. Real cells represent the cells that exist in the interior of the geometry, which are also the cells used in calculation process. The mesh of the model is shown in Fig. 2 and the total number of real cells of the model is 17,136, and there are 12 X cell lines, 12 Y cell lines and 119 Z cell lines. The gas mixture (fuel and N_2) is purged into the Fuel Reactor from the bottom and passes through the oxygen carrier bed. To eliminate the influence on the reaction rate of fuel partial pressure, the fuel partial pressure was set to 1 bar for all the cases, by adjusting the volume fraction of fuel in the gaseous mixture. During the simulation, the fuel reacts with the oxygen carrier. The fuel is

Table 1
Simulated cases.

	Case study	Validation 1	Validation 2	Sensitivity on Pressure	Sensitivity on Temperature
Fuel type	Syngas (50 % H_2 & 50 % CO)	H_2	CO	Syngas	Syngas
Fuel flow (m/s)	0.3	0.3	0.3	0.3	0.3
Temperature (K)	1073	1073	1073	1073	973, 1073, 1173, 1273
Pressure (bar)	10	1, 5, 10	1, 5, 10	1, 5, 10, 15 , 20	10

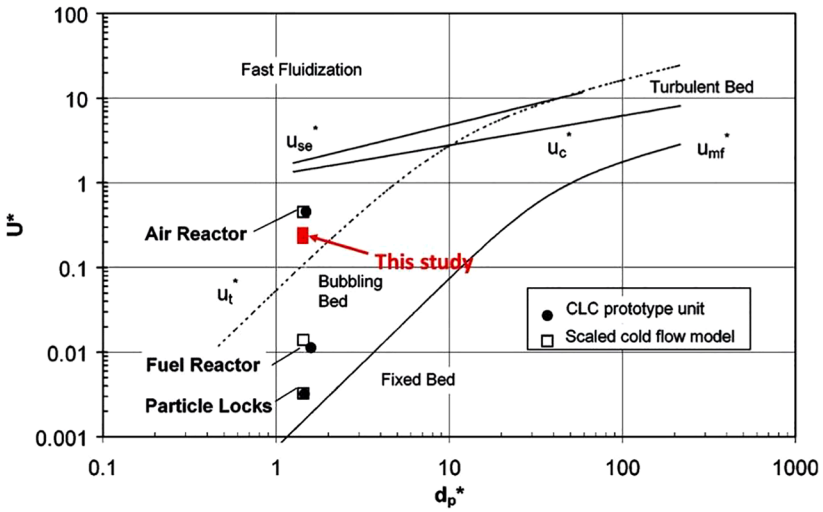

Fig. 3. Different operating regimes of air and fuel reactor, according to [40] and [41].

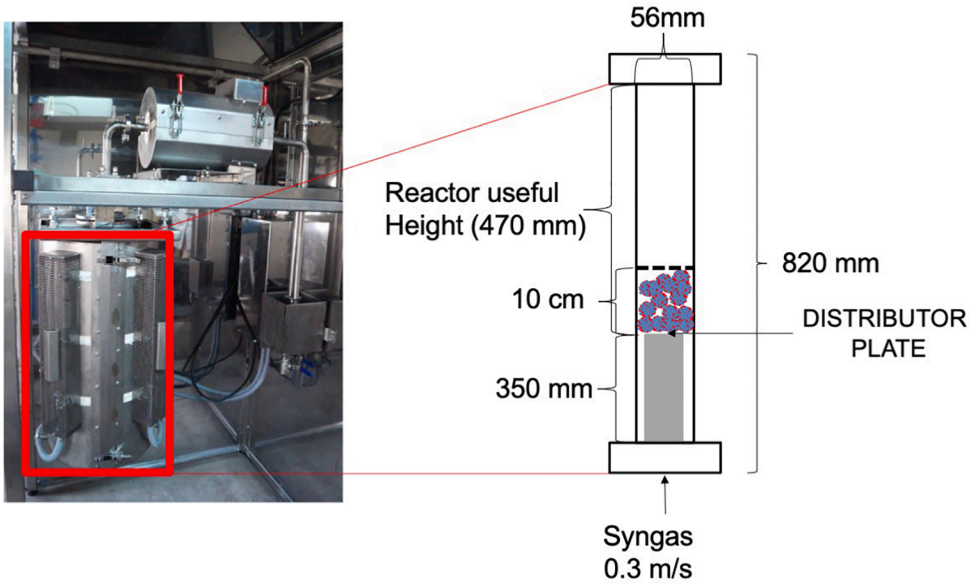

Fig. 4. Fluidized bed reactor configuration [32].

oxidized while the oxygen carrier is reduced. It is essential to control the operating conditions: like the flow rate of the fuel, to optimize the oxygen carrier fluidization. The detailed operating conditions are shown in Table 1. The outlet is located at the top of FR, which is set to: pressure boundary equal to 1 bar.

We can see from Table 1 that two separate validations of the model are performed, based on the experimental data reported in [26]: first the model is validated with hydrogen as a fuel (considering the experimental conditions in terms of flow and partial pressure reported in [26]) and then the model is validated for carbon monoxide (considering the experimental conditions in terms of flow and partial pressure reported in [26]). The approach adopted is possible, given that in the same experimental tests the two gases were treated first separately and then they were mixed (final results showed a good correspondece to the sum of the results obtained from the two separate gases).

2.2. Oxygen carrier properties and their influence on kinetics and thermodynamic aspects

Highly reactive Fe-based oxygen carrier supported by Al_2O_3 was studied. The main physical properties of the oxygen carrier are shown in Table 2. It contains 45 % of metal oxide, as indicated by the short name (Fe45Al) and it is prepared by freeze granulation. The characterization data were taken from the lab-scale analysis performed previously in ICB-CSIC studies [15,26]. Due to the different strength, reactivity, porosity and specific surface area of each oxygen carrier, the contents of the active metal (MeO) and particle size are different. Sphericity and solid volume fraction of the oxygen carriers were set to 0.85 and 0.6, respectively [36]. The initial oxygen carriers bed height was set as 100 mm, which is a typical value of the tests already performed at the lab facility.

To have a good computational performance of the simulation, as already said, a limited number of reactions for the oxygen carrier reduction are considered (see reactions (1) and (2)).

It is worth noting that iron can have several kinds of reduced forms (Fe_3O_4, FeO, Fe) but only the transformation between Fe_2O_3 and Fe_3O_4 may be applicable for industrial CLC systems [42]. Therefore, it has been imperative to control the state of iron oxide during the modeling process. This has been obtained by carefully estimating with the CFD software the time required to perform a reduction cycle.

Table 2
Oxygen carrier main physical properties and kinetic parameters for the reduction reaction [15,26].

	Active MeO content (wt. %)	Particle size (μm)	Kinetic parameters	k_o ($mol^{1-n}m^{3n-2}s^{-1}$)	E (kJ/mol)	n	d
Fe45Al	45	150	H_2	2.30E-3	24	0.8	−1.03
			CO	6.20E-4	20	1.0	−0.89

The chemical reaction rate is a function of temperature T, pressure P, the concentration C_i of gas evolved in the reaction and time t. It is measured from experimental data which have been empirically fitted based on the Shrinking Core model to derive Arrhenius law constants. The activation energy, pre-exponential factor and order of reaction have been then inserted in the Barracuda-VR^{TM} software, as shown in eq. (3). The detailed discussion on implementing these reactions can be found in Hamilton et al. [43].

$$\frac{dX_{MO}}{dt} = k_0 \left(\frac{P}{P_0}\right)^d e^{\frac{-E}{RT}} C_i^n \tag{3}$$

where $\frac{dX_{MO}}{dt}$ is the oxygen carrier conversion rate, k_0 is the pre-exponential constant, P_0 is atmospheric pressure, E is the activation energy, R is the universal gas constant. The detailed parameters used to model chemical reactions are shown in Table 2.

The data shown in Table 2 has been derived through the experiments described in [26]. The tests shown in [26] have mainly compared different oxygen carriers (Cu-, Ni- and Fe- based) using syngas as the reducing agent.

In these experiments total pressure has been changed between 0.1 and 3.0 MPa. The experiments were carried out with two approaches: at constant partial pressure of the reducing gas and at constant volume fraction of the fuel gas. Different sets of experiments were performed with separated H_2 and CO or with mixed H_2 and CO in different proportions. The grain model with spherical or plate-like geometry in the grains was chosen for the determination of the kinetic triplets and it was assumed that the chemical reactions controlled the global reaction rate (and so that gas diffusion into the oxygen carrier particle was negligible). The results of the experiments performed in [26] have shown interestingly that with Cu- and Fe- oxygen carriers the reaction rate of the oxygen carrier with syngas corresponded to the sum of the effects obtained using the individual fuel gases: CO and H_2. This is very important also for the study presented in the paper, because it confirms that the approach of validating the model separately with H_2 and CO it is correct, because then when adding the two effects in the final simulation at pressurized conditions, we will have a reasonable result. Other important results of the experiments are:

- the reaction rate of hydrogen is generally higher than that of CO, so in chemical looping combustion in pressurized conditions hydrogen confirms to be more reactive than carbon monoxide as a fuel;
- experimental analysis has shown that an increase in working pressure has a remarkable negative effect on the reaction rate of all the considered oxygen carriers and all the types of reactions (both reduction and oxidation);
- it was also noted that it is not possible to use the kinetic rate derived at atmospheric conditions to model what happens in pressurized conditions.

The solution to the discrepancy between kinetics at atmospheric conditions and kinetics at pressurized conditions was represented by an "apparent" pre-exponential factor described by Abad et al. 2007 [26] in the following way:

$$k_{0,p} = k_0 (P/P_0)^{pq} \tag{4}$$

where k_0 is the pre-exponential factor at atmospheric pressure and $k_{0,p}$ is the pre-exponential factor at pressurized conditions, P_0 is atmospheric pressure and P is the actual pressure of the experiments or the simulation, pq is the parameter calculated experimentally to relate the kinetics at atmospheric and pressurized conditions.

The oxygen carrier has also relevant impact on the thermodynamic aspects of the reduction reaction. First of all it is worth saying that by a thermodynamic point of view the sum of the two heats released in the air and in the fuel reactor should be equal to the heat of combustion of the fuel, as reported in [44]. This does not mean that both the heats are positive, in fact if the heat released in the air reactor is always positive, given that the oxidation reaction is always exothermic the reduction reaction can be either exothermic or endothermic it depends on the reduction enthalpy which is influenced by the type of oxygen carrier used and the type of fuel also. In the case of iron, as it can be seen in [8], the reduction enthalpy with Fe_2O_3 is positive with CH_4 (141.6 kJ/mol gas) while it is negative with CO (-47 kJ/mol gas) and H_2 (-5.8 kJ/mol gas). Negative enthalpy stays for exothermic processes, while positive enthalpy means endothermic processes. When Fe_2O_3 is used with syngas we see that the process is interestingly exothermic (so it is more favorable). When iron is supported over alumina (as in the present study) all the processes are exothermic. We have in fact a reduction enthalpy of −62.3 kJ/mol for CH_4, −56.8 kJ/mol for H_2 and −98.0 kJ/mol for CO. If we consider nickel based oxygen carriers, we can find quite a similar situation with iron. The reduction reaction is positive (156.5 kJ/mol of CH_4) with methane and negative for hydrogen and carbon monoxide (respectively −2.1 and −43.3 kJ/mol of gas). In the case of nickel this does not change with the support material, in fact we have the following reaction enthalpies: 158.6 kJ/mol with CH_4 and −1.6 kJ/mol with H_2 and −42.8 kJ/mol with CO; using $NiAl_2O_4$ as an oxygen carrier in the reduction reaction.

An interesting perspective on thermodynamics aspects is provide by the work of the Oak Ridge National Laboratory [45] this work builds up on a previous one published by McGlashan [11]. The key thermodynamic aspect in CLC is that both reduction and oxidation reaction happen at temperatures which are closer to equilibrium temperature respect to conventional combustion (i.e. the equilibrium temperature of conventional combustion is too high and not possible to reach also for material resistance problems). This has implications also in the choice of the oxygen carrier [11], in fact if we take iron, which has endothermic reduction reaction and exothermic oxidation reaction this has a higher second law efficiency because the difference in temperature between the two reactions could drive two heat engines and recover waste heat from the process.

2.3. *Barracuda-VR^{TM} modeling*

The hydrodynamics and heat transfer models adopted in this study have already been described in Reinking et al. [36]. The drag model used is WenYu-Ergun blended drag model developed by Beetstra et al. [46]. Turbulence is described by Large Eddy Simulation (LES) approach, and Smagorinsky subgrid-scale model is used by Barracuda-VR^{TM} [47]. The fluid-phase continuity equation and the momentum equation are:

$$\frac{\partial(\theta_f \rho_f)}{\partial t} + \nabla\cdot(\theta_f \rho_f \boldsymbol{\mu}_f) = \delta \dot{m}_p \tag{5}$$

$$\frac{\partial(\theta_f \rho_f \boldsymbol{\mu}_f)}{\partial t} + \nabla\cdot(\theta_f \rho_f \boldsymbol{\mu}_f \boldsymbol{\mu}_f) = -\nabla P - \boldsymbol{F} + \theta_f \rho_f \boldsymbol{g} + \nabla\cdot(\theta_f \boldsymbol{\tau}_f) \tag{6}$$

where θ_f and ρ_f are the volume fraction and density of the fluid, respectively. $\boldsymbol{\mu}_f$ is the velocity, $\boldsymbol{\tau}_f$ is the stress tensor, $\boldsymbol{F}$ is the momentum

exchange rate between the fluid and solid phase. g is gravitational acceleration, which is set to 9.80665 m/s^2. t is the time, $\delta\dot{m}_p$ is the fluid-mass source item that is generated by the reaction between the solid phase and the fluid phase.

2.3.1. Energy equation (enthalpy equation)

The energy conservation equation is shown in eq. (7).

$$\frac{\partial(\theta_f\rho_f h_f)}{\partial t}+\nabla\cdot(\theta_f\rho_f h_f\boldsymbol{\mu_f})=\theta_f\left(\frac{\partial p}{\partial t}+\boldsymbol{\mu_f}\cdot\nabla p\right)+\phi-\nabla\cdot(\theta_f q)+S_h+\dot{q}_D \quad (7)$$

h_f is the fluid enthalpy, p is the mean flow gas thermodynamic pressure. ϕ is the viscous dissipation. S_h represents the conservative energy exchange between the solid phase and the fluid phase and q is the fluid heat flux. The term q is calculated with the following equation:

$q = -(\lambda + \lambda_t)\nabla T_f$ (8).

Where:

- $\lambda + \lambda_t$ are the laminar and turbulent thermal conductivity;
- ∇T_f is the gradient of temperature.

On the other hand $\dot{q}_D$ is the enthalpy diffusion which is given by:

$$\dot{q}_D=\sum_{i=1}^{N_2}\nabla\cdot\left[h_i\theta_f\rho_f(D+D_t)\nabla Y_{f,i}\right] \quad (9)$$

Where:

- h_i is the enthalpy of the fluid species;
- θ_f is the fluid volume fraction;
- ρ_f is the fluid density;
- $D + D_t$ are the laminar and turbulent species diffusivity;
- $Y_{f,i}$ is the mass fraction of species i.

The approach adopted is consistent with that adopted in [48]. The wall to bed heat transfer coefficient is the one already present by default in the Barracuda® software, which is also consistent with the one adopted in [49].

2.3.2. Species transport equations

The species transport equation is reported as follows:

$$\frac{\partial(\theta_f\rho_f Y_{f,i})}{\partial t}+\nabla\cdot(\theta_f\rho_f Y_{f,i}\boldsymbol{\mu_f})=\nabla\cdot(D\theta_f\rho_f\nabla Y_{f,i})+\delta\dot{m}_{i,chem} \quad (10)$$

$Y_{f,i}$ represents the mass fractions of each gas species and D is the turbulent mass diffusivity related to the viscosity by Schmidt number correlation $\mu/\rho_f - D = Sc$ and Sc is set to 0.9.

2.3.3. Governing equations for solid phase

The particle phase behavior is predicted by solving a transport equation for the particle distribution function (PDF) f. Where f is a function of particle positionx_s, velocityu_s, massm_s, temperature T_s and time t:

$$\frac{\partial f}{\partial t}+\frac{\partial(fv)}{\partial x}+\frac{\partial(fA)}{\partial v}=\frac{f_D-f}{\tau_D} \quad (11)$$

f is the PDF for the local mass averaged particle velocity and τ_D is the collision damping time. A is the particle acceleration, which is determined by:

$$A=\frac{du_s}{dt}=D_s(u_f-u_s)-\frac{1}{\rho_s}\nabla p-\frac{1}{\theta_s\rho_s}\nabla\tau_s+g+Fs \quad (12)$$

D_s is the interphase momentum transfer coefficient which is a function of the particle size, velocity, position and time.θ_s, ρ_s and τ_s represent solid phase fraction, mass density and contact normal stress, respectively. Fs the particle friction per mass, which is only important at very low particle flow at near close pack.

To simplify the model, the wall of FR was assumed to be adiabatic and there is no oxygen carrier consumed by attrition. In a real Fuel Reactor, a small percentage of heat will be lost from the wall and also oxygen carriers will change their properties due to the processes happening in the bed, such as attrition and sintering, but also carbon deposition. The fact that the reactor is adiabatic allows us to model the reactor available in the laboratories of the Instituto de Carboquimica (ICB), belonging to the Consejo Superior de Investigaciones Cientifica (CSIC) see Fig. 4. This is a reactor realised in kanthal alloy and heated by electricl furnaces. The reactor configuration is shown in Fig. 4.

The settings chosen for heat transfer will allow to validate the model against previous experimental data derived from ICB-CSIC plants, even though further analysis will be needed on the process enthalpy characterization, to understand the amount of heat which will be released by the chemical reactions. This aspect will be further analyzed in the discussion section.

3. Model Validation

Model validation has been performed based on the rate of conversion of the oxygen carriers with pure reaction gases, so pure H_2 and pure CO. The use of pure and non-mixed syngas components was chosen because it is easier to directly control the effect of kinetic parameters on syngas single components (i.e. H_2 and CO) reaction rate; this approach was followed as indicated also already in Table 1. Fig. 5 shows the comparison between the calculational results and experimental results of Fe_2O_3 conversion at different pressures. Experimental results are derived from PTGA tests, reported in [26] and [50].

It can be seen that the calculated results are in good agreement with the experimental results, proving the validity of the model and of the kinetic parameters. The calculated results also show that the Fe_2O_3 conversion rate is slightly lower than experimental results. This can be explained with the fact that the fuel flow in the TGA experiments interests a very small mass, while in the case of the batch reactor we have less ratio between the mass of the fuel and that of the oxygen carrier (in particular this affects the C_i parameter in the eq. (3)). For CO fuel, the Fe_2O_3 conversion rate is slightly higher than the experimental results at 10 bars after 10 s. This is due to the fact that the conversion rate of Fe_2O_3 in the batch reactor is an averaged value on the whole reactor volume and it is affected by the turbulence of the airflow and other parameters involving heat exchange and temperature gradient formation. This eventually results in differences between the experimental data and the modelled ones which have no significance by a scientific point of view.

If the same flow as in the PTGA is used and the same partial pressure of the reacting gas is maintained, the results should be pretty comparable. We have to remember that kinetic control of the reaction predominates in the first part of the reaction, see [15]. So, we believe the assumption made is realistic.

4. Results

The results section is divided in 5 main parts which take into consideration:

- Temperature field description and insights on the heating rate;
- Fe_2O_3 particles volume fraction during time;
- Influence of pressure on the reduction reaction process in the Fuel Reactor;
- Influence of temperature on the reduction reaction in the Fuel Reactor;
- Syngas conversion efficiency in the Fuel Reactor.

The above-mentioned aspects will be described in detail in the following sections.

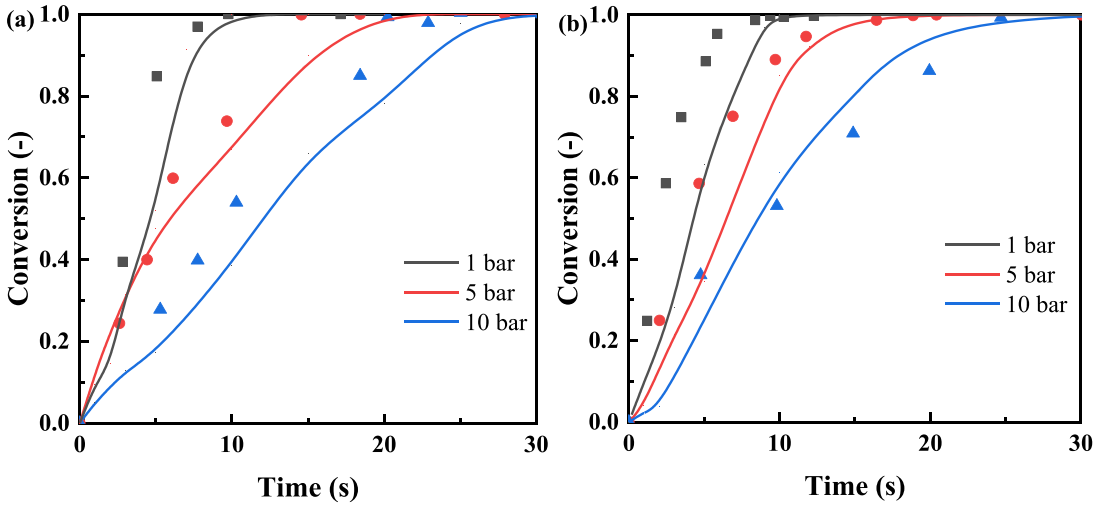

Fig. 5. Validation of Fe_2O_3 conversion process: a comparison between calculations and experiments using H_2 (a) and CO (b) as fuel at different pressures. Continuous lines represent calculated data; the dots represent TGA experimental data [50].

4.1. *Temperature field description and insights on the heating rate*

The data on the temperature fields in the reactor at 10 s of simulation, when the reaction is still happening, are shown in Fig. 6 and Fig. 7.

Fig. 6 shows the trend of temperature in the reactor at different temperatures. The higher the temperature the more is the difference between the temperature of the freeboard and the temperature of the bed, meaning that the bed has lower reactive behavior while it is the freeboard where the reactions happen. In fact, the gas enters the solids bed and transports the solids in the freeboard where they react faster. The reaction as we know is exothermic for what has been said in paragraph 2.2 about the oxygen carrier. In this sense the oxygen carrier bed shows to have a higher thermal inertia if compared with the freeboard.

On the other hand, we see interestingly from Fig. 7 that with the increase of the pressure the thermal inertia in the solids decreases, meaning that the heat transfer is improved. This can be explained with the fact that the bubbles inside the bed get smaller with the increase of the pressure, which will not only improve the heat and mass transfer, but also favor the gas hold-up and homogeneity in the FR [51]. This is a very interesting result on the effect of pressure on the temperature field inside the reactor when pressure is applied, which has been confirmed by previous experimental studies and simulation studies [51,52].

4.2. *Fe_2O_3 particles volume fraction during time*

In Fig. 8 it is shown the volume fraction of the Fe_2O_3 oxygen carrier in function of time. We can see from Fig. 8 how the oxygen carrier fluidizes under the effect of the syngas flow entering the reactor from the bottom. Bubbles firstly form at the bottom of the reactor and then rise as time goes on. When bubbles reach the surface of bed, they burst and result in the fluctuation of bed surface [53].

As the syngas enters from the bottom of the reactor, the oxygen carrier in the lower part reacts with it and is converted into Fe_3O_4. Because the reaction between the oxygen carrier and the syngas is fast, the syngas is almost consumed at the bottom of the reactor, so the oxygen carrier at the top is hardly transformed. Over time, the oxygen carrier at the bottom is consumed, and the oxygen carrier at the top begins to convert. According to the 0D simulation studies of

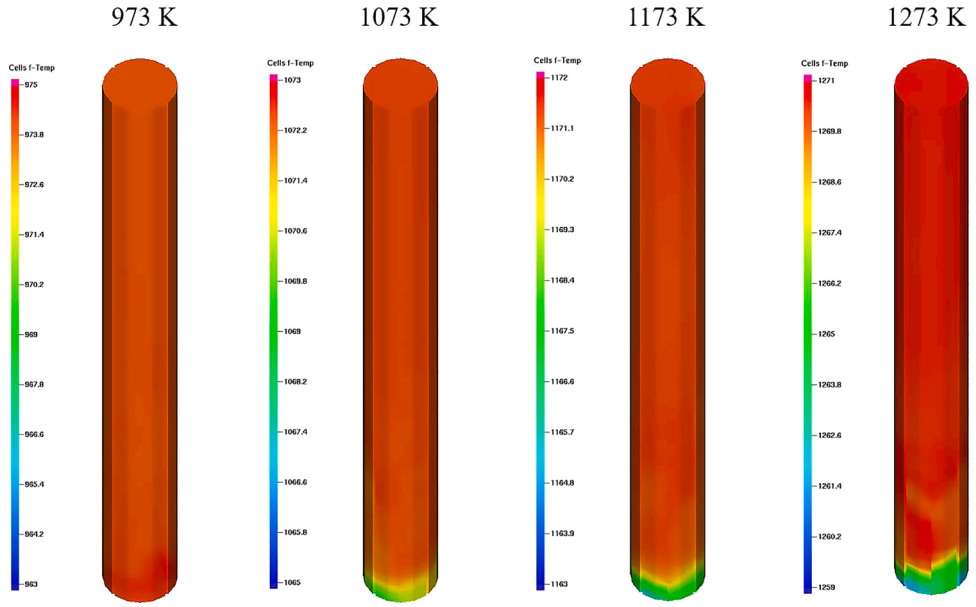

Fig. 6. Temperature fields of FR at different temperatures (10 s).

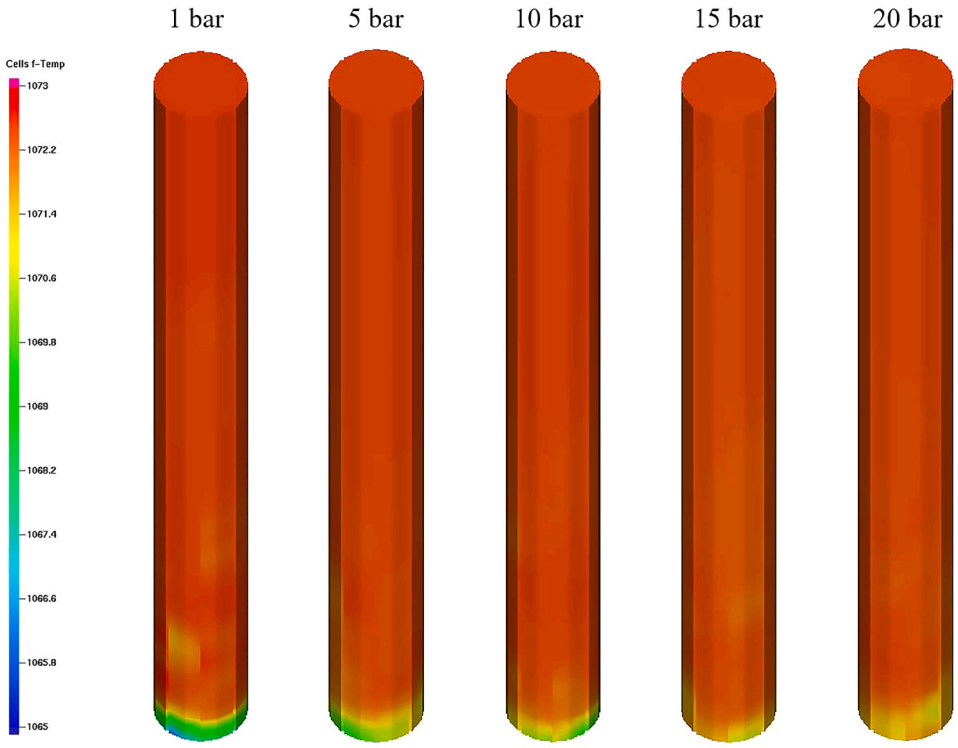

Fig. 7. Temperature fields of FR at different pressures (10 s).

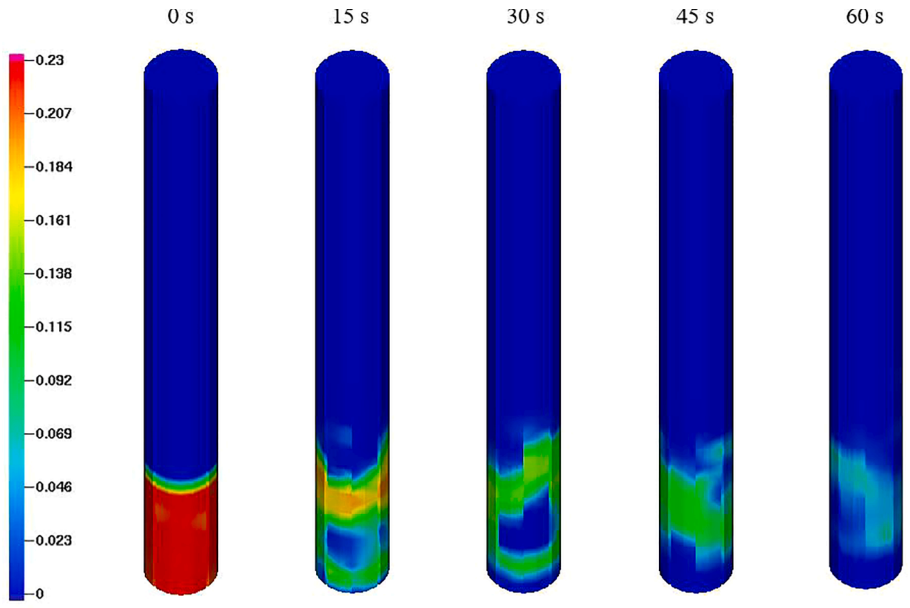

Fig. 8. Fe_2O_3 particle volume fraction during time (Syngas, 1073 K, 10 bar).

Hamidouche et al. [54] and Abad et al. [55], the reaction rate of fuel will decrease, due to inadequate contact of the OC with the fuel. Around 60 s, the OC has almost completely reacted; this will cause non-ideal combustion efficiency and implies a new reduction cycle has to be set in place. The average reduction cycle duration of 60 s also confirms what has been already reported in [32,54].

4.3. Influence of pressure on the reduction reaction process in the fuel reactor

Temperature is a fundamental parameter if we want to couple a gas turbine with a pressurized chemical looping combustor. The efficiency of the plant in fact depends on the Turbine Inlet Temperature (TIT). We want a target temperature close to 1200 °C but this is difficult to achieve in PCLC plants, so the combustor is optimized to work at a feasible temperature of about 1000 °C. We see from the results shown in Fig. 9 and Fig. 10 that the conversion of the gas is very efficient at that temperature and so the reactor design is correspondent to the specifications of a potential power plant. On the other had we have to consider also the effect of pressure which is the other parameter which derectly influnces the eficiency of the power plant.

Fig. 9 shows the volume fraction of Fe_2O_3 at 60 s under different

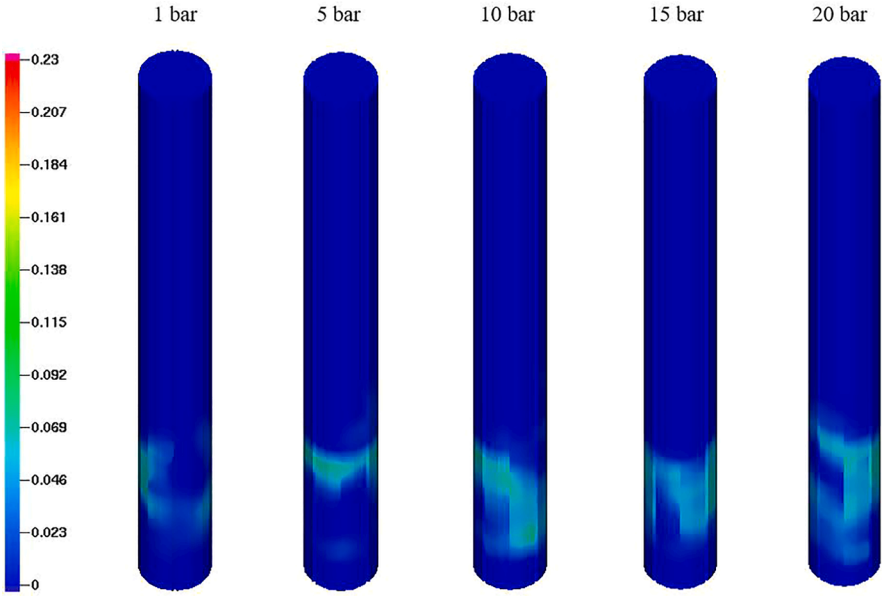

Fig. 9. Comparison of volume fraction of Fe_2O_3 at different pressures (time = 60 s).

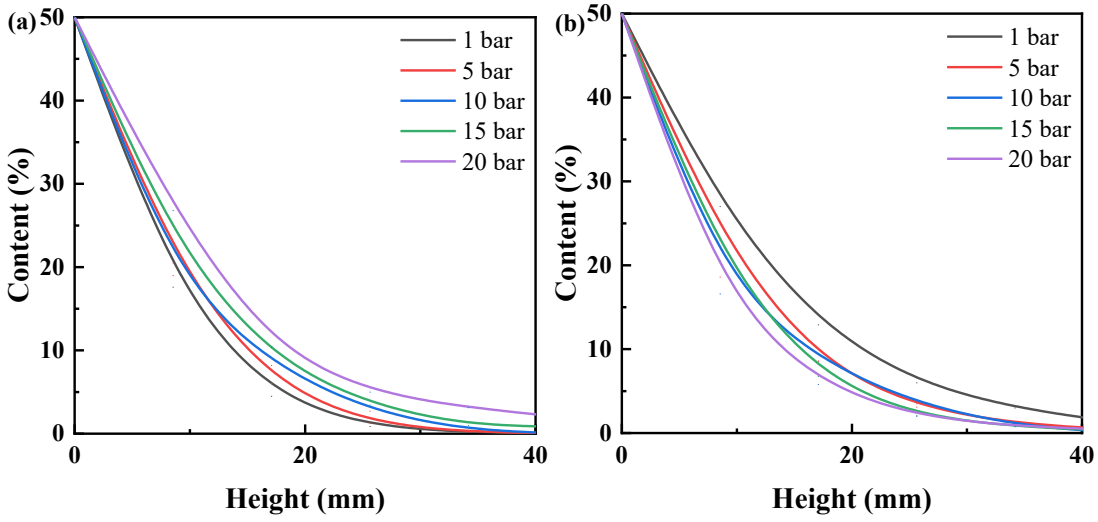

Fig. 10. Content of H_2 (a) and CO (b) at different reactor heights under different pressure (Syngas, 1073 K, 10 s).

pressures. With the increase of pressure, the volume fraction of Fe_2O_3 increases. This means that the reaction rate is less fast, which is consistent with the conclusion drawn by Abad et al. [50]. It is worth to notice that, the influence of pressure is stronger on the range of 1 bar to 10 bars than on the range from 10 bars to 20 bars. As pressure further increases, the influence on the reaction rate is weakened.

Fig. 10 shows the syngas (H_2 and CO) oxidation process through the height of the reactor under different pressures. It can be seen that, the H_2 conversion rate decreases with the increase of pressure. For the pressures of 1 bar and 5 bars, H_2 is almost completely transformed at 30 mm height. But as the pressure increases to 10 bars, H_2 is completely transformed at 40 mm height. As pressure further increases to 15 bars and 20 bars, the reaction rate is further reduced. At 40 mm, the H_2 concentrations are still ~ 1 % and ~ 3 %, respectively. Unlike H_2, CO shows an opposite trend as pressure changes. The CO concentration still has 2 % residue at 40 mm height under 1 bar, but as pressure increases, the CO is almost completely transformed, which is in contrast with the kinetic parameters calculated by the TGA tests performed in [50]. Based on previous studies [50,54–56], increasing pressure will decrease the reactivity between OCs and fuel. On the other hand increasing pressure will decreasing the size of the bubbles and favor the heat and mass transfer. Reaction rate depends on the competition between reactivity and heat and mass transfer. This is also the reason why the reaction rate changes trend for CO, as it is shown in Fig. 10. Previous studies on the influence of pressure on the reaction rate mostly used fixed beds [15,56], so heat and mass transfer had little influence on the reaction rate. The reason why H_2 and CO show different trends with the increase of temperature is mainly attributed to the fact that the reaction kinetic parameters of H_2 are more sensitive to pressure changes than those of CO. Therefore, as pressure increases, the dominant factor affecting H_2 conversion rate is kinetics, so its reaction rate decreases. For CO, heat transfer prevails on the effect of kinetics and this is improved by pressure (this is possible because the reactivity of H_2 is much higher than that of CO and so it does not allow to see the effect of heat transfer happening). Based on the decrease of conversion which has been noted in Fe_2O_3 as per Fig. 9, it can be concluded that the elevated pressure has more influence on H_2 than on CO.

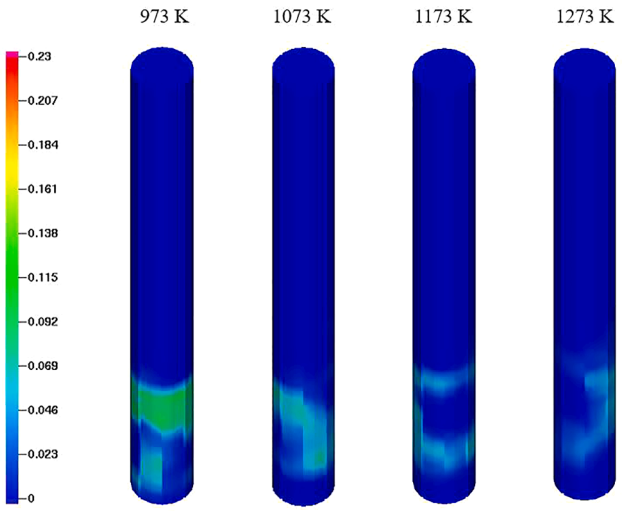

Fig. 11. Volume fraction of Fe_2O_3 at different temperatures (pressure = 10 bars, time = 60 s).

4.4. Influence of temperature on the reduction reaction in the fuel reactor

Since H_2 and CO both have good conversion rates at 10 bars, we studied the reduction process in the Fuel Reactor under different temperatures at 10 bars. It can be seen from Fig. 11 that the reaction rate clearly increases as temperature increases.

At 973 K, there is half of Fe_2O_3 residue at the top of bed at 60 s. As temperature increase to 1273 K, the amount of Fe_2O_3 has almost completely reacted. The syngas conversion process along the reactor height follows also a similar trend (as it can be seen from Fig. 12).

For temperature equal to 973 K, we can note there is a low reaction rate for syngas and the concentrations of both H_2 and CO are still equal to ~ 4v% at 40 mm height of the reactor. As temperature increases to 1037 K, the reaction rate increases considerably. H_2 and CO are almost completely converted at a height above 40 mm. As temperature further increases, the reaction rate increases also but the effect of temperature on the reaction rate is weakened. As it is known by common sense, it is beneficial to the stability of the reactor to reduce the operating temperature, while ensuring the fuel combustion efficiency. If the chemical looping combustor has to be coupled with a gas turbine there is also the need to have high temperature exhaust gases exiting it and entering the turbine inlet. Therefore, 1073 K is a worthwhile operation condition for the Fuel Reactor but if we have to couple it to a gas turbine at least 1273 K will be needed.

4.5. Syngas conversion efficiency in the fuel reactor

Fig. 13 and Fig. 14 show the concentration of syngas at the outlet of Fuel Reactor at a time when all the oxygen carrier has been consumed. At the time above ~ 70 s, the content of H_2 and CO at the outlet begins to increase and reaches again 50 v% for both gases at ~ 80 s. This means that at the 80th second the oxygen carrier has finished all the oxygen which can be transferred to the fuel for oxidizing it and so it is completely reduced. As the pressure increases, the time to complete reduction decreaes up to 10 bars; then with the increase of the pressure the conversion rate of the gas increases.

This is due in our opinion to the fact that the increase of pressure up to 10 bars has an effect on slowing the kinetics as confirmed also by the PTGA tests. On the other hand, the effect of pressure improves fluidization and produces smaller bubbles in the bed and increases heat transfer, so this effect increases the reaction rate at higher pressures for CO. The effect is seen only on CO because H_2 is converted much faster and this cannot be appreciated. Therefore, once the pressure is increased above 10 bars, this will speed up the conversion of Fe_2O_3. It is important to note that changes in temperature and pressure affect CO much more than H_2. This may be an important point to note for Fuel Reactor operation and design.

It can be seen from Fig. 15, that elevated pressures will increase the conversion rate of CO, which proceeds much slower than that of H_2 (which is more reactive). Fig. 15 confirms the fact that H_2 conversion rate is much more influenced by the effect of pressure and shows a decrease which is more evident than that of CO conversion rate and begins when the pressure is over 10 bars.

If we consider the total effect of pressure on syngas conversion at the outlet of the reactor we can see that the slower conversion rate due to a slower kinetics is not respected at the outlet of the reactor. We see that the heat exchange, due to the smaller dimensions of the bubbles, has the most important effect in this case. So finally the conversion efficiency of the syngas is improved by the increase of pressure in the batch reactor.

As the effect of elevated pressure on CO is much greater than H_2, elevated pressure is beneficial to the overall conversion efficiency of syngas. This also means that for this Fuel Reactor, the increase in pressure can influence also the ratio between fuel and oxygen carrier and the final inventory (expressed in kg of oxygen carrier per MW of syngas

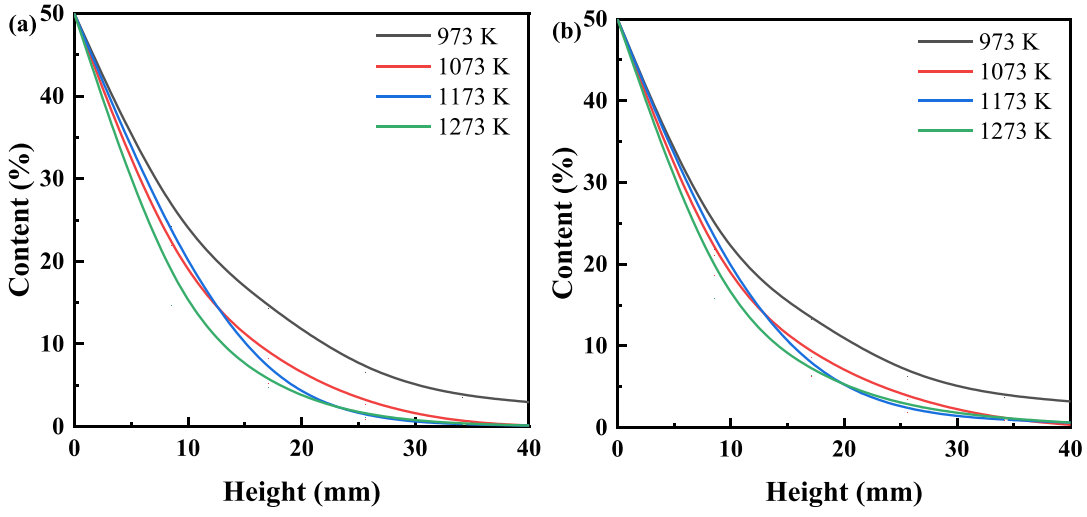

Fig. 12. The content of H_2 (a) and CO (b) at different reactor heights under different temperatures (Fuel = Syngas made of 50v% H_2 and 50v% CO, Pressure = 10 bars, Time = 10 s).

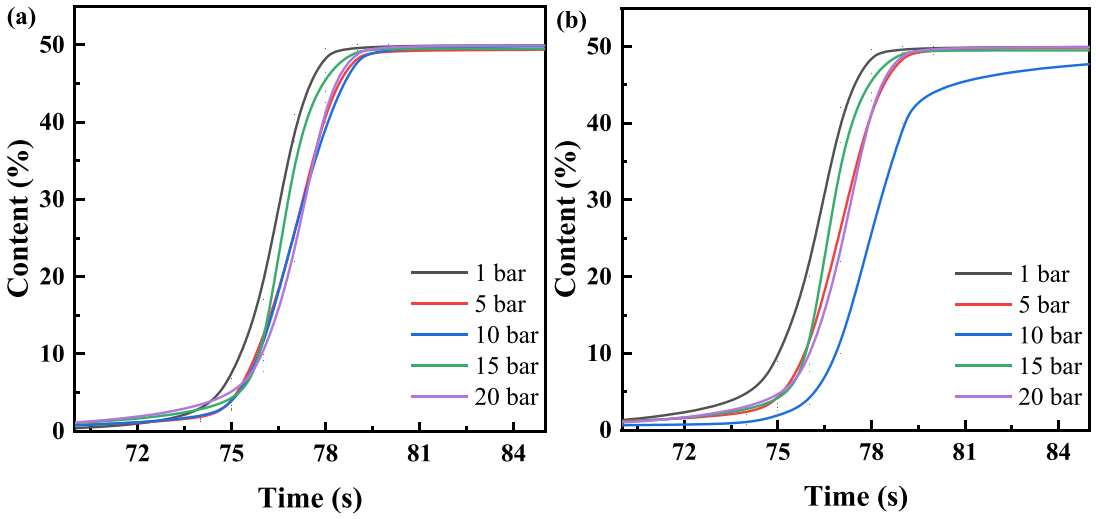

Fig. 13. Concentration of H_2 (a) and CO (b) at the outlet of the reactor under different pressures.

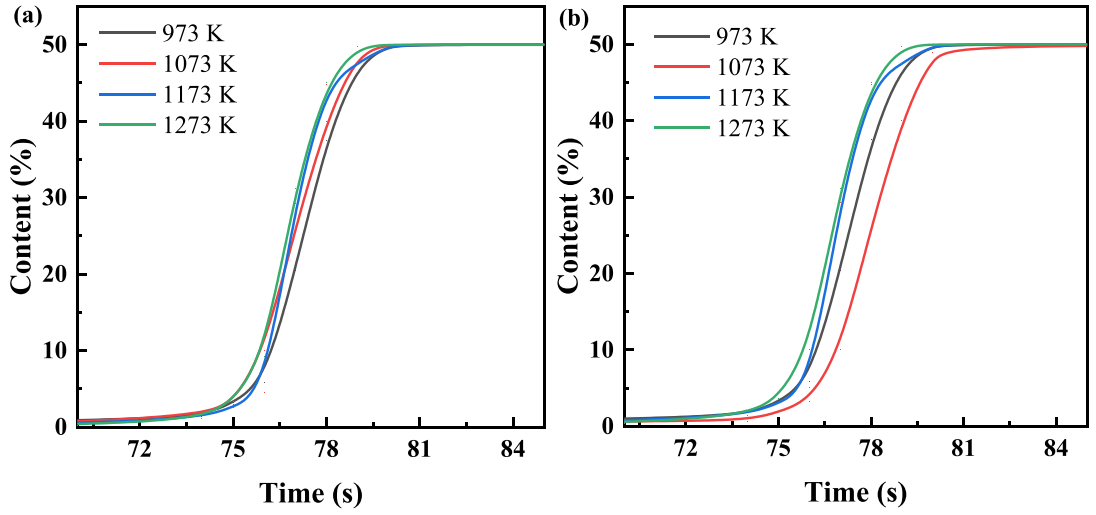

Fig. 14. Concentration of H_2 (a) and CO (b) at the outlet of the fuel reactor under different temperatures.

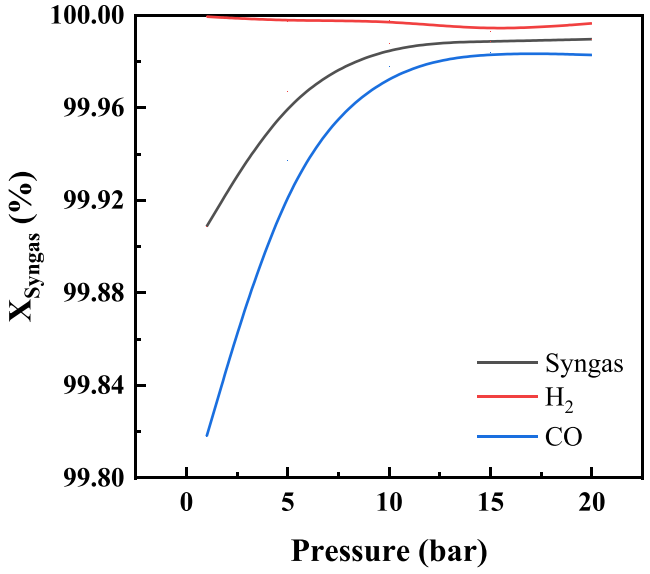

Fig. 15. Influence of pressure on the conversion efficiency of syngas in the Fuel Reactor.

input). Fig. 16 shows the amount of oxygen carrier required to achieve a syngas conversion rate equal to 99.9 % at different pressures. The required oxygen carrier bed height is linearly decreasing with the increase of pressure, the details are shown also in Table 3. At 20 bars, the amount of oxygen carriers required is only 64.9 % of that required at 1 bar, which is of great significance for designing the system.

Oxygen carrier is an important component of the CLC system, and its physicochemical properties are the key factors affecting the performance of CLC system. The PCLC system has important requirements on the physicochemical properties of the oxygen carriers. Since the reactivity of the oxygen carrier is inhibited by pressure, it is necessary to modify the catalyst to adapt it to the pressure conditions or explore new materials. In addition, the resistance to attrition, agglomeration and the stability of the oxygen carrier under pressurized conditions need to be further explored.

5. Discussion

5.1. Main insights on the effect of pressure on the reaction rate and syngas conversion in pressurized chemical looping combustion

This paper assesses the effects of pressure on syngas conversion

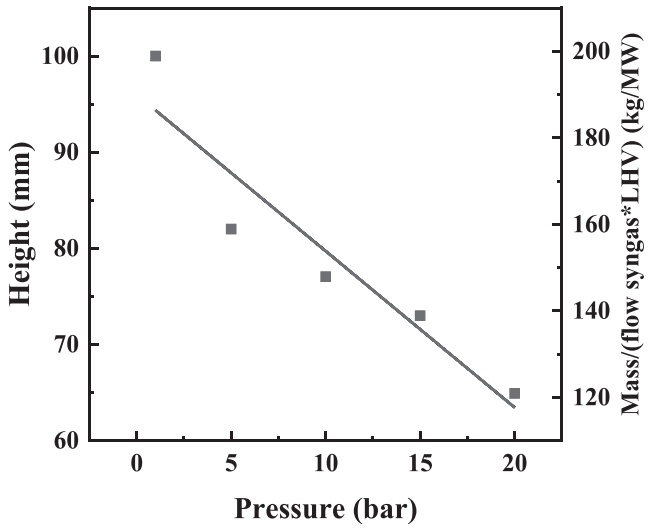

Fig. 16. Adaptations required to bed height to counteract the effect of pressure increase on oxygen carrier conversion rate.

Table 3
Details of the minimum amount of oxygen carrier required at different pressures to achieve 99.9% of syngas conversion.

Pressure	Height (mm)	Mass (kg)	Inventory (kg/MW)
1	100	1.72	198.71
5	82	1.41	162.89
10	77.06	1.33	153.65
15	72.99	1.26	145.56
20	64.9	1.08	124.77

efficiency and on oxygen carrier reaction rate. We started with the main results of the tests performed on a PTGA at the Instituto de Carboquimica (ICB) belonging to the Spanish National Research Council (CSIC) with different oxygen carriers and different working pressures. The main conclusions for these PTGA tests are shown in Table 4, together with the main insights about gas–solid reactions, derived from the previous experimental results and simulation results under pressurized conditions; as well as the main insights derived from the CFD analysis performed on the batch fluidized bed plant considered in this study (and also shown in Fig. 17).

5.2. Main insights on the design of pressurized chemical looping combustors to be coupled to gas turbines

Recalling the insights presented in Table 4, we see that an important conclusion is presented by the identification of the optimal inventory to work with in the particular fuel reactor, which was object of this study. Based on previous studies of the ICB-CSIC research group on combustion and gasification we see that we can have different values of the final inventory for different reactors.

As explained in [26] the kinetic data derived from PTGA analysis can have a practical use in the identification of the solid inventory, which is necessary to completely oxidize the fuel that is fed to the fuel reactor. The methodology developed by ICB-CSIC for this kind of calculation is based on the following assumptions:

- Perfect mixing of oxygen carrier particles;
- Plug flow behavior of the fuel gas;
- No resistance between the gas passing from bubble to emulsion phase in the fuel reactor;

Based on these assumptions the solid inventory can be calculated according to the following equation [63,64]:

Table 4
Comparison between the main insights obtained from PTGA and the main insights obtained by the CFD analysis.

ICB [26,57]	
Parameter	**PTGA behavior**
Solid conversion rate	- The solid conversion rate increases with temperature and syngas concentration. The reduction rate of the oxygen carrier is not influenced by the concentration of reduction products (H_2O and CO_2). The reactivity of the OC is influenced by the solid inventory used in the FR and needed to fully convert the syngas to H_2O and CO_2. The solids inventory necessary to combust H_2 are generally lower than those required to combust CO in the fuel reactor.
H_2 reaction rate	- The reactivity of the OC with hydrogen is usually higher than that with the CO. The reactivity of the OC in pressurized conditions depends strongly on the type of OC and cannot be modeled with kinetic parameters derived at atmospheric conditions.
CO reaction rate	- Solid conversion obtained with CO is much slower than that obtained with H_2. The reaction order for the CO reaction ($n = 1$) is higher than that of the H_2 reaction ($n = 0.8$), this implies that the reaction rate for carbon monoxide becomes lower at high conversion of the syngas, and this implies that the trend of conversion of CO decreases and is less fast than that of H_2 (as already said).
Syngas reaction rate	- Syngas reaction rate behavior depends on the type of oxygen carrier; In the case of iron based oxygen carrier the reaction rate of syngas is given by the sum of the reaction rate of H_2 and the reaction rate of CO.
Previous experimental results and simulation results under pressurized conditions	
Parameter	**CFD model**
H_2S reaction rate [58]	- Pressure has a negative effect on the sulfidation reaction.
SO_2 reaction rate [59]	- SO_2 reaction rate decreases when total pressure increases while partial pressure of SO_2 keeps constant; SO_2 reaction rate increases when partial pressure of SO_2 increases while total pressure keeps constant; Increasing the total pressure results in a smaller diffusion coefficient of SO_2; Increasing the partial pressure of SO_2 reduces the effectivity diffusivity of SO_2;
Sulfidation reaction of CaO [60]	- Increasing pressure has a negative effect on the combined calcination and sulfidation steps.
CO reaction rate [61]	- Increasing the CO partial pressure (at a constant total pressure) leads to higher rates of reaction and higher oxygen transport capacity; Increasing the total pressure (at a constant CO partial pressure) has the reverse effect.
Kinetics [62]	- The negative effect of the pressure on the redox kinetics is most probably caused by external mass transfer limitations.
Sulfidation rate [56]	- Sulfidation rate increases with total pressure when the volume fraction of H_2S is constant; Sulfidation reaction is controlled by the chemical reaction and diffusion together.
This study	
Parameter	**CFD model**
H_2 reactivity	- H_2 tends to react generally more quickly with the oxygen carrier and its conversion usually is very high at all the pressures which have been taken into account. With the increase of pressure H_2 reactivity tends to decrease. The maximum reduction of the reactivity of H_2 is in correspondence to the pressure of 10 bars, then with the increase of pressure the heat transfer rate and the properties of the bed influence positively the reaction rate.
CO reactivity	- The effect of pressure improves fluidization produces smaller bubbles in the bed and increases heat transfer so this effect increases the reaction rate at higher pressures

(*continued on next page*)

Table 4 (*continued*)

ICB [26,57] Parameter	PTGA behavior
	for CO. The effect is seen only on CO because H_2 is converted much faster and this cannot be appreciated. Therefore, once the pressure is increased above 10 bars, this will speed up the conversion of Fe_2O_3.
Syngas	- If we consider the total effect of pressure on syngas conversion at the outlet of the reactor we can see that the slower conversion rate due to a slower kinetics is not respected at the outlet of the reactor and that we finally see that the heat exchange due to the smaller dimensions of the bubbles has the most important effect in this case.
Temperature effect	- As noted for the PTGA experiments the increase in temperature tend to increase the speed of the reaction but this effect interacts deeply with that of pressure on kinetics and on the fluidization and heat transfer performance.

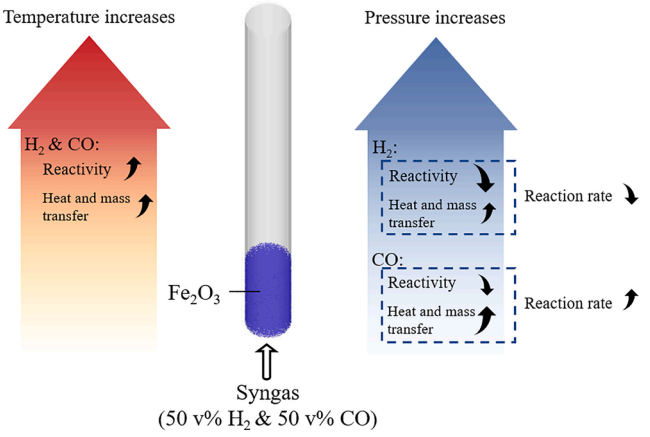

Fig. 17. The main insights derived from the CFD analysis performed on the batch fluidized bed plant.

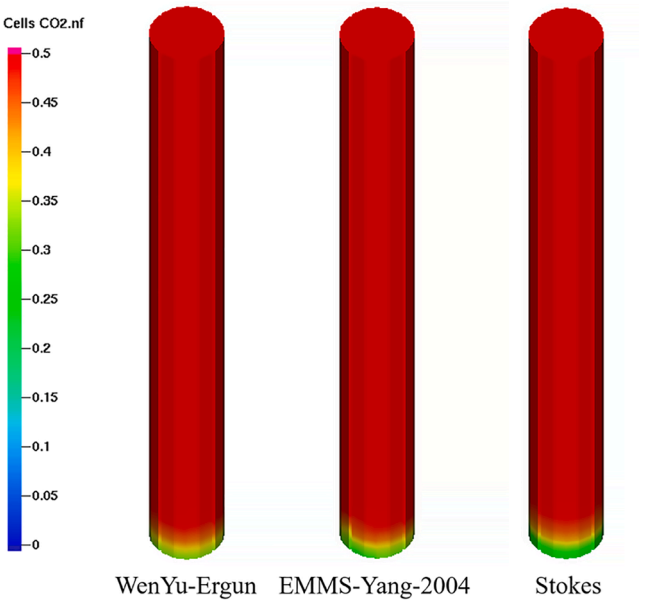

Fig. 18. Sensitivity analysis of different drag force models on CO_2 content (1073 K, 10 bars, 10 s).

$$m_{OC}^{*} = y_g \Delta X_g \frac{2dM_O}{R_{OC}\Delta H_c^{*}} \frac{\overline{\tau}}{\Phi} = y_g \Delta X \frac{2dM_O}{\Delta H_c^{0}} \frac{\delta}{\Phi(-\overline{r}_0)} \quad (13)$$

Where:

- m_{OC}* is the inventory mass per MW;
- y_g is the molar fraction of the gas;
- X_g is the gas conversion rate;
- d is the stoichiometric factor for the combustion of syngas with oxygen;
- M_O is the atomic weight of the oxygen;
- R_{OC} = is the oxygen transport capacity of the oxygen carrier;
- $\Delta H_c{}^0$ is the standard heat of combustion of the gas fuel, see also [65];
- $\overline{\tau}$ is the time for complete solid conversion for the reaction at $\overline{C}(s)$; where C is the gas average concentration;
- Φ is the characteristic reaction rate, as defined in [64];
- δ is obtained from the derivation of the equations used to describe the time for complete solid conversion, depending on the modeling approach which is chosen;
- $-r_0$ is equal to R_{OC}*(dX_r/dt), where X_r is the solid conversion in the reduction reaction.

Dealing with the calculation of time for complete solid conversion, this is done based on eq. (14) if we speak about spherical grain geometry; or eq. (15) if we speak about plate-like geometry:

$$\frac{1}{\tau} = 1 - (1 - X_r)^{1/3} \quad (14)$$

$$\frac{1}{\tau} = X_r \quad (15)$$

Following the assumptions made in [26] we derive a value for the inventory needed to oxidize completely H_2 of about 15 kg/MW at 1 bar and a value of 30 kg/MW at 20 bars. While for syngas we would obtain about 31 kg/MW if WGS equilibrium is not considered and 30 kg/MW if WGS equilibrium is considered. We see from this data that the solids inventory increases with the increase in pressure, this contradicts again the results of the CFD analysis presented in this work. But can be easily explained with the fact that in reality when working with a batch fluidized bed which has a significant mass of the oxygen carrier, the behavior of the bed has an important effect. This means that in general we need more inventory that what calculated with the PTGA, in the real conditions represented by a fuel reactor (see what reported in Table 3). Besides this an important conclusion of our study is that when considering the effect of pressure on the fluid dynamics and heat transfer using a Eulerian-Lagrangian method and a LES method for modeling turbulence, it appears that the behavior of the bed, the temperature gradient and the heat transfer are the final parameters that influences the rate of conversion of the syngas, more than the chemical kinetics.

This important information is not the only one we need to perform a detailed design of the plant, which is proposed in the GTCLC-NEG project. In fact, we need also:

- information on the oxygen carrier circulation rate, as reported in [64];
- information of the oxidation and reduction enthalpies, which are different for the different types of oxygen carriers, see what reported in [65].

If we put together the information about the kinetics, the heat and mass transfer, the solids inventory, the solids circulations rates, the mass flows of fuel and air, the heat integration and the different enthalpies of the different steps which compose the cycle that can be obtained by coupling a PCLC reactor with a gas turbine we can optimize the plant as a whole. This kind of plants has been already proposed for example by the MIT, see the publication on the design and optimization of a

chemical looping combustion power plant with CO_2 capture, proposed in [66]. Or the wok on pressurized chemical looping combustion developed at Canmet ENERGY [61]. Or the works on the optimization of such plants performed at TOTAL, see [67]. From many studies it seems that such power plants [68–70] will pay a significant penalty in terms of energy efficiency respect to conventional NGCC power plants and conventional coal power plants [71–77].

For this reason, the GTCLC-NEG project aims at developing an approach for the design of such plants granting high heat integration between the reactors and so high plant final efficiency.

5.3. Sensitivity analysis on drag force

The sensitivity analysis on the drag force model is proposed in Fig. 18. Three approaches have been compared: the Wen-Yu-Ergun correlation [78,79], the EMMS-Yang-2004 [80] and the Stokes approach [81].

The three approaches considered give good agreement among the obtained results.

6. Conclusion

A three-dimensional model based on the MP-PIC method was developed to investigate the performance of a Fuel Reactor using Fe_2O_3 as oxygen carrier and syngas as fuel under elevated pressures. The syngas flow is calculated based on LES turbulent model and oxygen carrier particles are tracked with DEM. The dynamics of the particle phase is described by a transport equation. Particle-scale chemical reactions are considered on the grid cell based on DEM.

Through the simulation of the Fuel Reactor at different pressures and temperatures and under elevated pressure conditions (10 bars), the behaviors of Fe_2O_3 oxygen carrier and syngas are effectively predicted. The conversion rate of Fe_2O_3 has good consistence with experimental results. The results demonstrate that elevated pressure inhibits the reactivity of Fe_2O_3 but favors the heat and mass transfer. Increasing pressure promotes the reaction of CO and Fe_2O_3 and inhibits the reaction of H_2 and Fe_2O_3. This is due to the fact that the heat and mass transfer of the reaction between CO and Fe_2O_3 is greatly affected by elevated pressure, and this prevails on the kinetics effect. Dealing with H_2 this has an opposite behavior, respect to CO, because it is highly reactive and the effect of heat and mass transfer is negligible, respect to the effect of the kinetics. Overall, the elevated pressure promotes the reaction between syngas and Fe_2O_3 and reduces the demand for the oxygen carrier in the system. Increasing the temperature not only promotes the reactivity, but also the heat and mass transfer in the FR. CO is more affected by pressure changes and temperature changes than H_2, which reveals to us an important insight for Fuel Reactor design and optimization. Before realizing the large-scale industrial utilization of PCLC, the influence of pressurized conditions on the reduction and oxidation characteristics of OCs still needs to be further explored. Besides, modifying OCs to adapt to pressurized conditions or seeking new OCs that have excellent performance under pressurized conditions may become a hot spot in future research.

Declaration of Competing Interest

The authors declare that they have no known competing financial interests or personal relationships that could have appeared to influence the work reported in this paper.

Data availability

Data will be made available on request.

Acknowledgments

This work has been funded by the GTCLC-NEG project that has received funding from the European Union's Horizon 2020 research and innovation programme under the Marie Sklodowska-Curie grant agreement No. 101018756. Special Acknowledgments are given to Dr. William A. Rogers of the National Energy Technology Laboratory (US) for helping in the concluding remarks on the arrangements needed to carefully model the effect of pressure on the PCLC plant.

Data Availability

please refer to the following repository/community of the project in ZENODO: https://zenodo.org/communities/gtclc-neg/?page=1&size=20

References

[1] Yamagata Y, Hanasaki N, Ito A, Kinoshita T, Murakami D, Zhou QJSS. Estimating water–food–ecosystem trade-offs for the global negative emission scenario (IPCC-RCP2. 6). 2018;13(2):301-13.
[2] Porrazzo R, White G, Ocone R. Techno-economic investigation of a chemical looping combustion based power plant. Faraday Discuss 2016;192:437–57.
[3] M. Siddi The European Green Deal: Assessing its current state and future implementation 2020.
[4] Sikora A. European Green Deal – legal and financial challenges of the climate change. ERA Forum 2021;21(4):681–97.
[5] Song T, Shen L. Review of reactor for chemical looping combustion of solid fuels. Int J Greenhouse Gas Control 2018;76:92–110.
[6] Adánez J, Abad A, Mendiara T, Gayán P, de Diego LF, García-Labiano F. Chemical looping combustion of solid fuels. Prog Energ Combust 2018;65:6–66.
[7] O'Neill BC, Kriegler E, Riahi K, Ebi KL, Hallegatte S, Carter TR, et al. A new scenario framework for climate change research: the concept of shared socioeconomic pathways. Clim Change 2013;122(3):387–400.
[8] Adanez J, Abad A, Garcia-Labiano F, Gayan P, de Diego LF. Progress in Chemical-Looping Combustion and Reforming technologies. Prog Energy Combust Sci 2012;38(2):215–82.
[9] Shao Y, Agarwal RK, Wang X, Jin B. Review of Computational Fluid Dynamics Studies on Chemical Looping Combustion. J Energy Res Technol 2021;143(8).
[10] Kruggel-Emden H, Stepanek F, Munjiza A. A Study on the Role of Reaction Modeling in Multi-phase CFD-based Simulations of Chemical Looping Combustion. Oil & Gas Science and Technology – Revue d'IFP Energies nouvelles 2011;66(2):313–31.
[11] McGlashan N. Chemical-looping combustion—a thermodynamic study. Proceedings of the Institution of Mechanical Engineers, Part C: J Mechan Eng Sci 2008;222(6):1005-19.
[12] Lyngfelt A, Leckner B. A 1000MWth boiler for chemical-looping combustion of solid fuels – Discussion of design and costs. Appl Energy 2015;157:475–87.
[13] Idziak K, Czakiert T, Krzywanski J, Zylka A, Kozlowska M, Nowak W. Safety and environmental reasons for the use of Ni-, Co-, Cu-, Mn- and Fe-based oxygen carriers in CLC/CLOU applications: An overview. Fuel 2020;268:117245.
[14] Petrakopoulou F, Boyano A, Cabrera M, Tsatsaronis GJIJoGGC. Exergoeconomic and exergoenvironmental analyses of a combined cycle power plant with chemical looping technology. 2011;5(3):475-82.
[15] Cabello A, Abad A, García-Labiano F, Gayán P, de Diego LF, Adánez J. Kinetic determination of a highly reactive impregnated Fe_2O_3/Al_2O_3 oxygen carrier for use in gas-fueled Chemical Looping Combustion. Chem Eng J 2014;258:265–80.
[16] Mayer K, Penthor S, Pröll T, Hofbauer HJAE. The different demands of oxygen carriers on the reactor system of a CLC plant–Results of oxygen carrier testing in a 120 kWth pilot plant. 2015;157:323-9.
[17] Mendiara T, Abad A, de Diego LF, García-Labiano F, Gayán P, Adánez J. Biomass combustion in a CLC system using an iron ore as an oxygen carrier. Int J Greenhouse Gas Control 2013;19:322–30.
[18] Gayán P, Pans MA, Ortiz M, Abad A, Luis F, García-Labiano F, et al. Testing of a highly reactive impregnated Fe_2O_3/Al_2O_3 oxygen carrier for a SR–CLC system in a continuous CLC unit. 2012;96:37-47.
[19] Piepers H, Cottaar EJE, Verkooijen A, Rietema KJPT. Effects of pressure and type of gas on particle-particle interaction and the consequences for gas—solid fluidization behaviour. 1984;37(1):55-70.
[20] Xiao R, Chen L, Saha C, Zhang S, Bhattacharya SJIJoGGC. Pressurized chemical-looping combustion of coal using an iron ore as oxygen carrier in a pilot-scale unit. 2012;10:363-73.
[21] Shimizu T. Pressurized fluidized bed combustion (PFBC). Fluidized Bed Technologies for Near-Zero Emission Combustion and Gasification. Elsevier 2013:669–700.
[22] Jin H, Ishida M. Reactivity Study on Natural-Gas-Fueled Chemical-Looping Combustion by a Fixed-Bed Reactor. Ind Eng Chem Res 2002;41(16):4004–7.
[23] Wolf J, Anheden M, Yan J. Comparison of nickel- and iron-based oxygen carriers in chemical looping combustion for CO_2 capture in power generation. Fuel 2005;84(7):993–1006.
[24] Rana S. Pressurized Chemical Looping Combustion of Natural Gas with Ilmenite for SAGD Application: An Oxidation Kinetic Study and Preliminary Air Reactor Model. Université d'Ottawa/University of Ottawa 2018.

[25] Ebrahimi-Kahrizsangi R, Abbasi MH. Evaluation of reliability of Coats-Redfern method for kinetic analysis of non-isothermal TGA. Trans Nonferrous Metals Soc China 2008;18(1):217–21.
[26] Abad A, García-Labiano F, de Diego LF, Gayán P, Adánez J. Reduction Kinetics of Cu-, Ni-, and Fe-Based Oxygen Carriers Using Syngas (CO + H_2) for Chemical-Looping Combustion. Energ Fuel 2007;21(4):1843–53.
[27] Liu Q, Zhong W, Yu A. Oxy-fuel combustion behaviors in a fluidized bed: A combined experimental and numerical study. Powder Technol 2019;349:40–51.
[28] Alobaid F, Almohammed N, Massoudi Farid M, May J, Rößger P, Richter A, et al. Progress in CFD Simulations of Fluidized Beds for Chemical and Energy Process Engineering. Prog Energ Combust 2022;91:100930.
[29] Ariyaratne WK, Manjula EVPJ, Ratnayake C, Melaaen M. CFD Approaches for Modeling Gas-Solids Multiphase Flows – A Review. 2016.
[30] Wang S, Lu H, Zhao F, Liu G. CFD studies of dual circulating fluidized bed reactors for chemical looping combustion processes. Chem Eng J 2014;236:121–30.
[31] Li S, Shen Y. Multi-fluid modelling of hydrodynamics in a dual circulating fluidized bed. Adv Powder Technol 2020;31(7):2778–91.
[32] Bartocci P, Abad A, Cabello A, de las Obras Loscertales M, Lu W, Yang H, et al. CFD Modelling of the Fuel Reactor of a Chemical Loping Combustion Plant to Be Used with Biomethane. Processes 2022;10(3):588.
[33] Li C, Eri Q. Comparison between two Eulerian-Lagrangian methods: CFD-DEM and MPPIC on the biomass gasification in a fluidized bed. Biomass Convers Bior 2021.
[34] Andrews MJ, O'Rourke PJJIJoMF. The multiphase particle-in-cell (MP-PIC) method for dense particulate flows. 1996;22(2):379-402.
[35] Snider DM, O'Rourke PJ. The multiphase particle-in-cell (MP-PIC) method for dense particle flow. Computational gas-solids flows and reacting systems: theory, methods and practice. IGI Global 2011:277–314.
[36] Reinking Z, Shim H-S, Whitty KJ, Lighty JS. Computational simulation of a 100 kW dual circulating fluidized bed reactor processing coal by chemical looping with oxygen uncoupling. Int J Greenhouse Gas Control 2019;90:102795.
[37] Zeng J, Xiao R, Zhang S, Zhang H, Zeng D, Qiu Y, et al. Identifying iron-based oxygen carrier reduction during biomass chemical looping gasification on a thermogravimetric fixed-bed reactor. Appl Energy 2018;229:404–12.
[38] Hallberg P, Jing D, Rydén M, Mattisson T, Lyngfelt A. Chemical Looping Combustion and Chemical Looping with Oxygen Uncoupling Experiments in a Batch Reactor Using Spray-Dried $CaMn1–xMxO_3–\delta$ (M = Ti, Fe, Mg) Particles as Oxygen Carriers. Energy Fuels 2013;27(3):1473–81.
[39] Mattisson T, García-Labiano F, Kronberger B, Lyngfelt A, Adánez J, Hofbauer H. Chemical-looping combustion using syngas as fuel. Int J Greenhouse Gas Control 2007;1(2):158–69.
[40] Kronberger B, Lyngfelt A, Löffler G, Hofbauer H. Design and fluid dynamic analysis of a bench-scale combustion system with CO_2 separation– chemical-looping combustion. Ind Eng Chem Res 2005;44(3):546–56.
[41] Bi HT, Grace JR. Flow regime diagrams for gas-solid fluidization and upward transport. Int J Multiph Flow 1995;21(6):1229–36.
[42] Mendiara T, Pérez R, Abad A, De Diego L, García-Labiano F, Gayán P, et al. Low-Cost Fe-Based Oxygen Carrier Materials for the i G-CLC Process with Coal. 1. 2012;51(50):16216-29.
[43] Hamilton MA, Whitty KJ, Lighty JS. Incorporating Oxygen Uncoupling Kinetics into Computational Fluid Dynamic Simulations of a Chemical Looping System. Energy Technology 2016;4(10):1237–46.
[44] Jerndal E, Mattisson T, Lyngfelt A. Thermal Analysis of Chemical-Looping Combustion. Chem Eng Res Des 2006;84(9):795–806.
[45] Chakravarthy VK, Daw CS, Pihl JA. Thermodynamic analysis of alternative approaches to chemical looping combustion. Energy Fuels 2011;25(2):656–69.
[46] Beetstra R, van der Hoef MA, Kuipers JAM. Numerical study of segregation using a new drag force correlation for polydisperse systems derived from lattice-Boltzmann simulations. Chem Eng Sci 2007;62(1–2):246–55.
[47] Smagorinsky J. General Circulation Experiments with the Primitive Equations. Mon Weather Rev 1963;91(3):99–164.
[48] Breault RW, Monazam ER. Modeling of the reduction of hematite in the chemical looping combustion of methane using barracuda. Energy Technology 2016;4(10):1221–9.
[49] Zhang Y, Wei Q. CPFD simulation of bed-to-wall heat transfer in a gas-solids bubbling fluidized bed with an immersed vertical tube. Chem Eng Process Process Intensif 2017;116:17–28.
[50] García-Labiano F, Adánez J, de Diego LF, Gayán P, Abad A. Effect of Pressure on the Behavior of Copper-, Iron-, and Nickel-Based Oxygen Carriers for Chemical-Looping Combustion. Energ Fuel 2005;20(1):26–33.
[51] Mansourpour Z, Karimi S, Zarghami R, Mostoufi N, Sotudeh-Gharebagh R. Insights in hydrodynamics of bubbling fluidized beds at elevated pressure by DEM–CFD approach. Particuology 2010;8(5):407–14.
[52] Song J, Liu D, Ma J, Chen X. Effect of elevated pressure on bubble properties in a two-dimensional gas–solid fluidized bed. Chem Eng Res Des 2018;138:21–31.
[53] Wang X, Jin B, Zhong W. Three-dimensional simulation of fluidized bed coal gasification. Chem Eng Process Process Intensif 2009;48(2):695–705.
[54] Hamidouche Z, Masi E, Fede P, Simonin O, Mayer K, Penthor S. Unsteady three-dimensional theoretical model and numerical simulation of a 120-kW chemical looping combustion pilot plant. Chem Eng Sci 2019;193:102–19.
[55] Abad A, Adánez J, García-Labiano F, de Diego LF, Gayán P. Modeling of the chemical-looping combustion of methane using a Cu-based oxygen-carrier. Combust Flame 2010;157(3):602–15.
[56] Song Z, Zhang M. Sulfidation Experiments in a Pressurized Thermogravimetric Analyzer With Chinese Calcined Limestones. 2005:27-35.
[57] Garcia-Labiano F, Adánez J, de Diego LF, Gayán P, Abad A. Effect of pressure on the behavior of copper-, iron-, and nickel-based oxygen carriers for chemical-looping combustion. Energy Fuels 2006;20(1):26–33.
[58] Agnihotri R, Chauk SS, Misro SK, Fan L-S. High-Pressure Reaction Kinetics of Hydrogen Sulfide and Uncalcined Limestone Powder. Ind Eng Chem Res 1999;38(10):3802–11.
[59] Qiu K, Lindqvist O. Direct sulfation of limestone at elevated pressures. Chem Eng Sci 2000;55(16):3091–100.
[60] Chauk SS, Agnihotri R, Jadhav RA, Misro SK, Fan LS. Kinetics of high-pressure removal of hydrogen sulfide using calcium oxide powder. AIChE J 2000;46(6):1157–67.
[61] Lu X, Rahman RA, Lu DY, Ridha FN, Duchesne MA, Tan Y, et al. Pressurized chemical looping combustion with CO: Reduction reactivity and oxygen-transport capacity of ilmenite ore. Appl Energy 2016;184:132–9.
[62] Pio MAS, Gallucci F, Roghair I, van Sint AM. Gas-solids kinetics of CuO/Al2O3 as an oxygen carrier for high-pressure chemical looping processes: The influence of the total pressure. Int J Hydrogen Energy 2017;42(17):12111–21.
[63] García-Labiano F, de DIEGO LF, Adánez J, Abad A, Gayán P. Reduction and oxidation kinetics of a copper-based oxygen carrier prepared by impregnation for chemical-looping combustion. Ind Eng Chem Res 2004;43(26):8168–77.
[64] Abad A, Adánez J, García-Labiano F, Luis F, Gayán P, Celaya J. Mapping of the range of operational conditions for Cu-, Fe-, and Ni-based oxygen carriers in chemical-looping combustion. Chem Eng Sci 2007;62(1–2):533–49.
[65] Adanez J, Abad A, Garcia-Labiano F, Gayan P, Luis FJPie, science c. Progress in chemical-looping combustion and reforming technologies. 2012;38(2):215-82.
[66] Iloeje CO, Zhao Z, Ghoniem AF. Design and techno-economic optimization of a rotary chemical looping combustion power plant with CO_2 capture. Appl Energy 2018;231:1179–90.
[67] Yazdanpanah M, Forret A, Gauthier T. Impact of size and temperature on the hydrodynamics of chemical looping combustion. Appl Energy 2015;157:416–21.
[68] Petriz-Prieto MA, Rico-Ramirez V, Gonzalez-Alatorre G, Gómez-Castro FI, Diwekar UM. A comparative simulation study of power generation plants involving chemical looping combustion systems. Comput Chem Eng 2016;84:434–45.
[69] Chiesa P, Lozza G, Malandrino A, Romano M, Piccolo V. Three-reactors chemical looping process for hydrogen production. Int J Hydrogen Energy 2008;33(9):2233–45.
[70] Thon A, Kramp M, Hartge E-U, Heinrich S, Werther J. Operational experience with a system of coupled fluidized beds for chemical looping combustion of solid fuels using ilmenite as oxygen carrier. Appl Energy 2014;118:309–17.
[71] Zerobin F, Pröll T. Potential and limitations of power generation via chemical looping combustion of gaseous fuels. Int J Greenhouse Gas Control 2017;64:174–82.
[72] Surywanshi GD, Patnaikuni VS, Vooradi R, Kakunuri M. CO_2 capture and utilization from supercritical coal direct chemical looping combustion power plant – Comprehensive analysis of different case studies. Appl Energy 2021;304:117915.
[73] Ogidiama OV, Abu-Zahra MRM, Shamim T. Techno-economic analysis of a poly-generation solar-assisted chemical looping combustion power plant. Appl Energy 2018;228:724–35.
[74] Hanak DP, Kolios AJ, Manovic V. Comparison of probabilistic performance of calcium looping and chemical solvent scrubbing retrofits for CO_2 capture from coal-fired power plant. Appl Energy 2016;172:323–36.
[75] Sorgenfrei M, Tsatsaronis G. Design and evaluation of an IGCC power plant using iron-based syngas chemical-looping (SCL) combustion. Appl Energy 2014;113:1958–64.
[76] Rajabi M, Mehrpooya M, Haibo Z, Huang Z. Chemical looping technology in CHP (combined heat and power) and CCHP (combined cooling heating and power) systems: A critical review. Appl Energy 2019;253:113544.
[77] Zhou L, Duan L, Anthony EJ. A calcium looping process for simultaneous CO_2 capture and peak shaving in a coal-fired power plant. Appl Energy 2019;235:480–6.
[78] Wen CY. Mechanics of fluidization. Chem Eng Prog Symp Ser 1966;62:100–11.
[79] Ergun S. Fluid flow through packed columns. Chem Eng Prog 1952;48:89–94.
[80] Ge W, Li J. Physical mapping of fluidization regimes—the EMMS approach. Chem Eng Sci 2002;57(18):3993–4004.
[81] Shearer SA, Hudson JR. Fluid mechanics: stokes' law and viscosity. Measurement Laboratory 2008;:3.